ACCURAY DEFORMABLE IMAGE REGISTRATION: DESCRIPTION AND EVALUATION

Petr Jordan, Andriy Myronenko, Kevin Gorczowski, Mark Foskey, Rich Holloway, Calvin R. Maurer, Jr.
Accuray Incorporated

Accuray Precision®

OVERVIEW

The concept of medical image registration[1,2] involves the task of spatial alignment of medical images, so that information from multiple scan dates or multiple modalities can be interpreted in a common coordinate system. The most widely used form of image registration involves the assumption of rigid transformation between a primary and a secondary dataset.

A more recent trend in medical image processing and in radiation therapy is the increasing adoption of deformable image registration (DIR)[3]. In DIR the transformation between images is assumed to be elastic, enabling alignment of anatomical differences that result from factors such as daily variation, patient position, immobilization, and respiratory phase. The applications of DIR in radiation therapy are broad, including multi-modal fusion for contouring on secondary scans (e.g., MR and PET), adaptive therapy, 4D planning[4], dose summation and tracking, retreatment, and multi-atlas autosegmentation[6-9]. This white paper describes the Accuray DIR algorithm, which has demonstrated excellent performance in a variety of applications.

ALGORITHM DESCRIPTION

The Accuray DIR algorithm is a fast multi-modal method capable of accurate non-rigid image registration between a wide range of imaging modalities. Internal experience from product development evaluation activities and external collaborations have shown good registration accuracy across a wide range of imaging modalities and anatomical site applications. Good spatial registration accuracy can be achieved even in challenging clinical applications, such as inter-fraction abdominal DIR, involving large daily variations in abdominal organ position and shape [9].

The algorithm is used for multi-atlas DIR in three automatic anatomy segmentation tools in the Accuray Precision® Treatment Planning System: Brain AutoSegmentation™ (based on T1w MR), Head & Neck AutoSegmentation™ (based on CT), and Male Pelvis AutoSegmentation™ (based on CT). The algorithm is also used in three image registration applications: PreciseART® Adaptive Radiation Therapy (to register CT-MVCT), PreciseRTX® Retreatment (to register CT-CT), and Deformable Image Registration (to register CT-MR and CT-CT and help with organ delineation).

The algorithm uses a nonparametric non-rigid transformation to represent the deformation field. It assumes no specific parameterization of the transformation; instead it explicitly estimates the deformation field subject to smoothness regularization. Such an approach allows estimating even complex organ deformations. Accuray DIR optimizes the similarity criterion, local Normalized Correlation Coefficient (NCC),

$$NCC(I_{ref}, I_{mov}) = \frac{\sum_{x,y,z}(I_{ref}(x,y,z) - \bar{I}_{ref})(I_{mov}(x,y,z) - \bar{I}_{mov})}{\sqrt{\sum_{x,y,z}(I_{ref}(x,y,z) - \bar{I}_{ref})^2}\sqrt{\sum_{x,y,z}(I_{mov}(x,y,z) - \bar{I}_{mov})^2}}$$

where $\bar{I}_{ref}$ is the reference image neighborhood patch and I_{mov} is the "moving" image neighborhood patch. $\bar{I}_{ref}$ and $\bar{I}_{mov}$ are the mean values of the volume patch. The similarity criterion is defined over small neighborhood patches, which allows for robust image matching even in the presence of intensity inhomogeneities and artifacts. The image similarity criterion is optimized iteratively over the entire image domain in a multi-resolution, coarse-to-fine scheme. The estimated deformation field is regularized using a smoothing operator at each iteration. Typical application uses 3 to 4 resolution levels and up to 500 iterations at each level. The algorithm is implemented using the nVidia CUDA GPU framework and is highly parallelized. A CT/MR deformable registration using a 300x300x300 voxel region of interest can be completed in 9 seconds on production GPU hardware (nVidia Quadro M5000).

In the DIR module of the Accuray Precision Treatment Planning System, the user can choose between low, medium, and high deformation smoothing settings. Medium smoothing is the default and recommended setting for most clinical applications. The high smoothing setting imposes more rigid regularization of the deformation field, making it more suitable for datasets with limited contrast to noise ratio or low spatial resolution. The low smoothing setting allows more flexibility in the deformation field, making it more suitable for datasets exhibiting very large deformations.

APPLICATIONS

THORACIC 4D CT DEFORMATION

Thoracic CT data was obtained from the publicly available POPI dataset[10], which includes six manually annotated 4D CT lung cases. Each lung case includes multiple 3D CT images at different respiratory phases. For the purpose of this study we only used a pair of end-exhale and end-inhale CT images from each case. Use of respiratory motion extrema provides the largest challenge for the DIR algorithm due to maximum separation between corresponding landmarks. An example of end-exhale and end-inhale lung images is shown in Figure 1. Each 3D CT image has approximately 100 manually placed ground-truth anatomical landmarks at different features of interest (evenly spread out over the lung volume).

The anatomical landmark mean registration error, across the six cases, were 8.1 ± 4.8 mm for the original 4D CT scans and 0.9 ± 0.9 mm after registration with Accuray DIR algorithm. The per-case landmark registration errors before and after deformable registration are summarized in Table 1. These results demonstrate a substantial improvement over a state-of-the-art academic implementation with a reported mean landmark error of 1.4 ± 1.5 mm [10] and commercial implementations with reported mean landmark errors of 3.0 ± 7.5 mm[11] and 1.5 ± 2.3 mm[12].

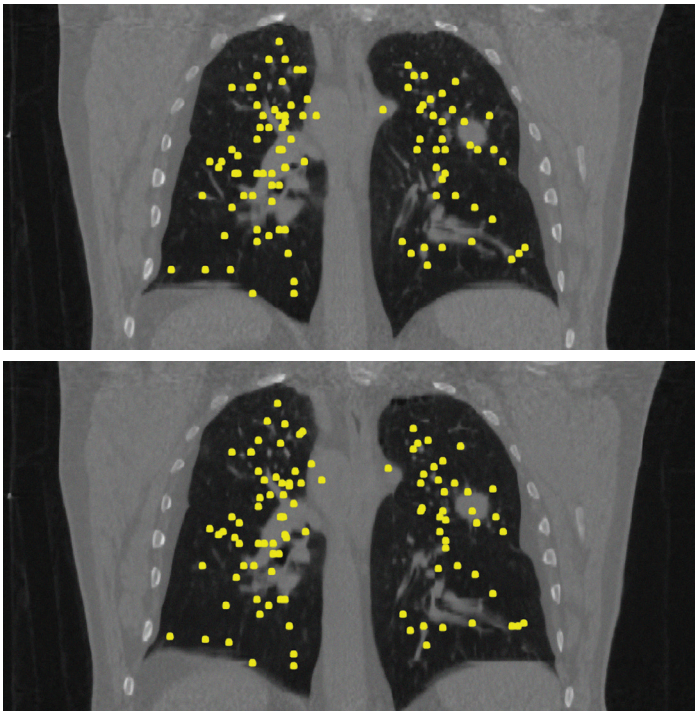

Figure 1. *Example of anatomical landmarks manually annotated in end-exhale (top) and end-inhale (bottom) phase of the POPI thoracic 4D CT dataset.*

Table 1. *Anatomical landmark agreement distance agreement before and after deformable registration.*

POPI Case	**Original 4D CT** Anatomical Landmark Distance (mm)		**Deformed 4D CT** Anatomical Landmark Distance (mm)	
	Mean	STD	Mean	STD
1	5.9	2.7	0.8	0.3
2	14.0	7.2	1.2	1.0
3	7.7	5.1	0.8	1.5
4	7.3	4.9	0.8	1.3
5	7.1	5.1	1.0	0.9
6	6.7	3.7	0.9	0.5
Mean	8.1	4.8	0.9	0.9

ABDOMINAL CT / MR DEFORMATION

Abdominal MR to CT DIR for liver tumor delineation is one of the most common and challenging applications of DIR in radiation therapy. We evaluated 10 cases with liver tumors defined on secondary MR scan, in terms of liver surface and internal fiducial agreement between primary CT and deformed secondary T1w MR scan. Liver contours were independently delineated on CT and MR scans by an expert radiation oncologist. Additionally, internal fiducial markers in the proximity of the treatment target were manually identified in all CT and MR scans. An example of ground-truth liver contours is shown in Figure 2. The majority of images were acquired at 1.56 x 1.56 x 1.00 mm CT resolution, and 1.18 x 1.18 x 3 mm MR resolution. All except one case (case 4) included at least three implanted fiducial markers.

In the first stage, an intensity-based rigid registration using a liver region of interest was performed to eliminate translation and rotation of the whole liver. In the second stage, the secondary T1w MR scan was registered to the primary CT using the Accuray DIR algorithm.

We compute initial error statistics for local rigid liver registration (as a reference) and for deformable registration performed over the entire abdominal region. In each case we compute the Dice coefficient, the mean fiducial distance, and the mean surface distance. More specifically, we compute the mean three-dimensional surface distance, that is, for each sample point on the CT contour surface, we find the closest point on the corresponding MR contour surface, producing a set of point-wise distances over which the mean surface distance is computed.

Based on the 10 liver cases analyzed, the initial (rigid) mean liver surface error was 1.82 mm, which decreased after DIR to 1.35mm. It should also be noted that a significant fixed component of the reported surface errors after registration is due to inherent uncertainty in CT/MR expert contours[5]. The mean liver Dice coefficient increased from 0.95 (rigid) to 0.97 (DIR), and the mean internal fiducial error between CT and deformed MR scans decreased from 3.26 mm (rigid) to 0.78 mm (DIR). The results of the evaluation are summarized in Table 2.

Based on visual inspection, the DIR algorithm significantly improved MR to CT alignment, with not only liver, but all organs and anatomical structures within the abdomen. Figure 3 shows an example of a typical abdominal CT/MR DIR result, significantly improving overall organ alignment compared to rigid registration.

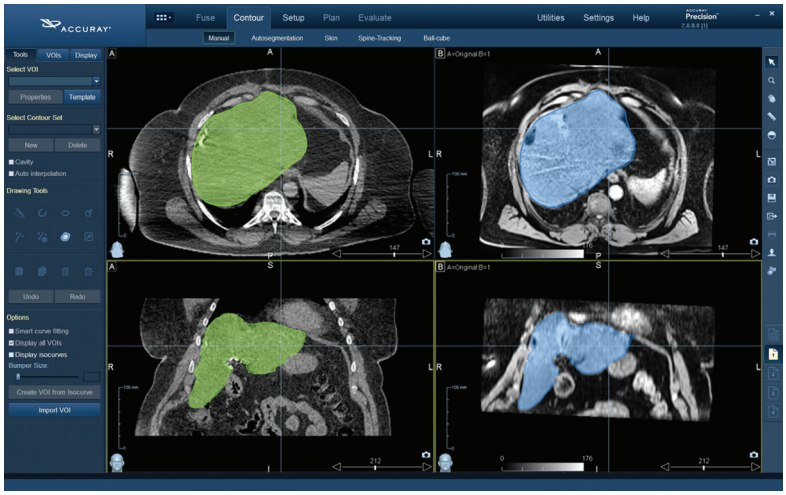

Figure 2. *Example of liver ground-truth contours. Contours drawn on CT shown in green (left), contours drawn on MR shown in blue (right).*

Table 2. *CT vs. MR liver contour and fiducial distance agreement using local rigid and deformable registration.*

Case	Local Rigid Registration			Deformable Registration		
	Mean Surface Distance [mm]	Dice	Mean Fiducial Error [mm]	Mean Surface Distance [mm]	Dice	Mean Fiducial Error [mm]
1	1.93	0.88	3.95	1.05	0.94	1.14
2	1.76	0.96	2.50	1.14	0.98	0.79
3	1.56	0.96	2.34	1.37	0.97	0.85
4	1.74	0.96	-	1.41	0.98	-
5	2.01	0.95	3.37	1.51	0.97	0.54
6	2.36	0.94	4.51	1.48	0.97	0.87
7	1.50	0.96	3.16	1.35	0.97	0.62
8	1.72	0.95	4.12	1.54	0.96	0.65
9	1.71	0.95	3.00	1.42	0.96	0.82
10	1.99	0.94	2.35	1.27	0.97	0.77
Mean	**1.82**	**0.95**	**3.26**	**¬1.35**	**0.97**	**0.78**

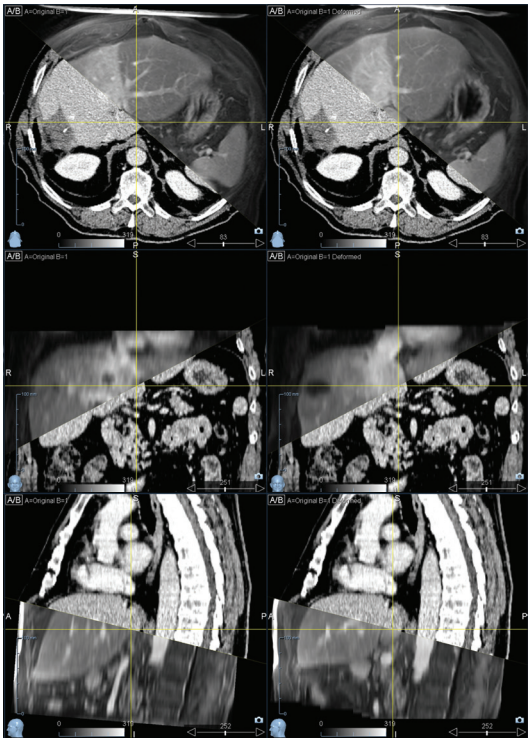

Figure 3. *Example of local rigid alignment (left) vs. whole abdomen deformable registration (right).*

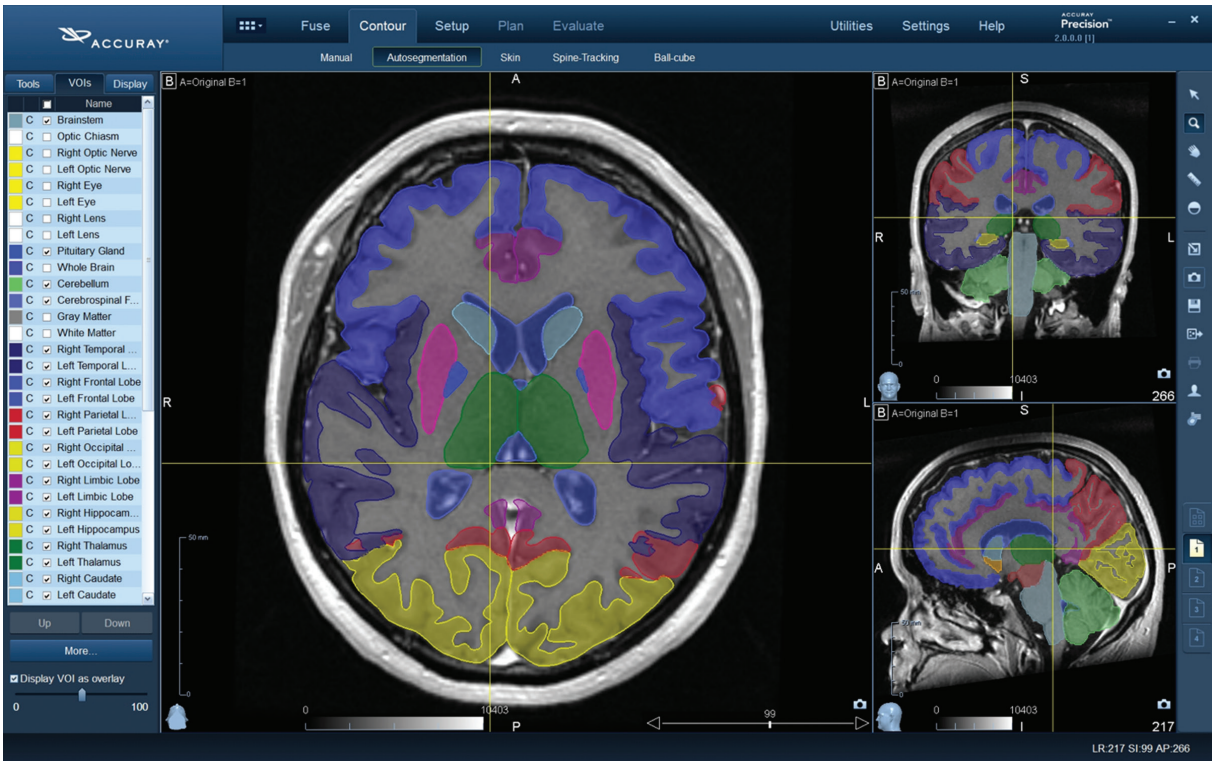

Figure 4. *Brain AutoSegmentation™ in Accuray Precision Treatment Planning System using deformation of expert atlases to patient T1w MR scan.*

MR BRAIN AUTOSEGMENTATION

Multi-atlas automatic organ delineation[6-9] is an important application of the Accuray DIR algorithm. The Brain AutoSegmentation (shown in Figure 4) was evaluated in terms of mean 3D surface error using leave-one-out analysis on expertly delineated datasets (N=20). An expertly delineated dataset containing 139 anatomical brain regions is visually compared to the autosegmentation result in Figure 5. While the expert dataset is estimated to require up to 4 days of neuroanatomist contouring time, the corresponding autosegmentation contours can be generated in approximately 3 minutes in the Accuray Precision Treatment Planning System with no user input, parameter selection, or initialization. The autosegmentation algorithm selects and deforms 20 morphologically most similar brain atlases. Subsequently, the deformed atlases are fused using a voting scheme to estimate a final consensus multi-atlas segmentation. The overall mean surface error between autosegmented structures and expert ground-truth segmentations is primarily composed of two sources of error: deformable registration error and atlas contouring uncertainty.

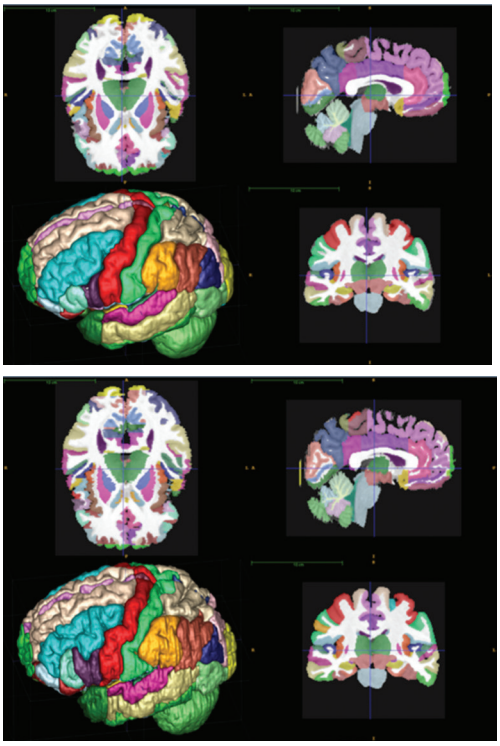

Figure 5. *Results of Brain AutoSegmentation (top) showing 139 anatomical regions vs. ground-truth manual segmentation (bottom) performed by a neuroanatomist.*

A leave-one-out analysis study was performed by independently evaluating one of 20 expert atlases as an autosegmentation case with known ground-truth, while using the remaining 19 atlases for multi-atlas autosegmentation. The analysis results (shown in Table 3) demonstrate mean anatomical accuracy of 0.5 mm for central brain structures and 0.9 mm for cortical brain structures. Critically important structures for radiation therapy, such as brainstem and optic chiasm, can be autosegmented with mean surface error as low as 0.3 mm.

Table 3. *Accuracy of MR Brain AutoSegmentation structures vs. ground-truth in terms of surface distances in leave-one-out analysis (N=20).*

Anatomical Structure	Mean Surface Error ± SD (mm)
All Central Brain Structures	0.5 ± 0.1
All Cortical Brain Structures	0.9 ± 0.1
Brainstem	0.3 ± 0.0
Optic Chiasm	0.3 ± 0.2
Thalamus	0.4 ± 0.1
Hippocampus	0.5 ± 0.3
Amygdala	0.4 ± 0.1
Accumbens	0.4 ± 0.1
Caudate	0.4 ± 0.2
Putamen	0.3 ± 0.0
Pallidum	0.3 ± 0.0
Ventral Diencephalon	0.3 ± 0.0
Precentral Gyrus	0.9 ± 0.5
Postcentral Gyrus	1.1 ± 0.5
Inferior Temporal Gyrus	0.9 ± 0.3
Middle Temporal Gyrus	0.9 ± 0.3
Superior Temporal Gyrus	0.9 ± 0.5
Transverse Temporal Gyrus	0.9 ± 1.0

CT HEAD & NECK AUTOSEGMENTATION

Analogous to the MR Brain AutoSegmentation™ study in the previous section, a leave-one-out analysis using 36 expert Head & Neck CT atlases was performed using the Head & Neck AutoSegmentation™. An example of automatically generated contours is shown in Figure 6.

Mean 3D surface errors between autosegmentation and ground-truth expert delineations are summarized in Table 4. These results demonstrate that the Accuray DIR algorithm enables accurate autosegmentation of Head & Neck anatomy in CT scans, as part of an algorithm achieving sub-millimeter mean autosegmentation accuracy for many structures, including whole brain, mandible, spinal cord and canal, globes, lenses, and optic nerves. Soft tissue structures with higher contouring uncertainty[14] due to limited CT contrast, including optic chiasm, larynx, and parotids, resulted in mean surface errors of 1.3 mm, 1.3 mm, and 1.6 mm respectively.

Table 4. *Accuracy of CT Head & Neck AutoSegmentation structures vs. ground-truth in terms of surface distances in leave-one-out analysis (N=36).*

Anatomical Structure	Mean Surface Error ± SD (mm)
Whole Brain	0.4 ± 0.1
Brainstem	1.0 ± 0.4
Mandible	0.5 ± 0.2
Spinal Cord	0.7 ± 0.2
Spinal Canal	0.7 ± 0.2
Globes	0.5 ± 0.2
Lenses	0.5 ± 0.2
Optic Nerves	0.6 ± 0.1
Optic Chiasm	1.3 ± 0.3
Larynx	1.3 ± 0.6
Parotids	1.6 ± 0.6
Precentral Gyrus	0.9 ± 0.5
Postcentral Gyrus	1.1 ± 0.5
Inferior Temporal Gyrus	0.9 ± 0.3
Middle Temporal Gyrus	0.9 ± 0.3
Superior Temporal Gyrus	0.9 ± 0.5
Transverse Temporal Gyrus	0.9 ± 1.0

Figure 6. *Results of Head & Neck AutoSegmentation™ using deformation of expert atlases to patient CT scan.*

ACKNOWLEDGEMENTS
Clinical images and liver delineations were graciously provided by Dr. Jakub Cvek (Fakultni Nemocnice Ostrava, Czech Republic).

REFERENCES

[1] Maintz JBA, Viergever MA. "A survey of medical image registration." Med Image Anal, 1998, 2(1), 1-36.

[2] Fitzpatrick JM, Hill DLG, Maurer CR Jr. "Image registration." In: Sonka M, Fitzpatrick JM, eds. Handbook of Medical Imaging, Volume 2: Medical Image Processing and Analysis. Bellingham, WA: SPIE Press, 2000, 447–513.

[3] Sotiras A, Davatzikos C, Paragios N. "Deformable Medical Image Registration: A Survey." IEEE Trans Med Imaging, 2013, 32(7), 1153–1190.

[4] West JB, Park J, Dooley JR, Maurer CR Jr.. "4D Treatment Optimization and Planning for Radiosurgery with Respiratory Motion Tracking." In: Urschel HC, Kresl JJ, Luketich JD, Papiez L, Timmerman RD, eds Robotic Radiosurgery: Treating Tumors that Move with Respiration. Berlin: Springer-Verlag, 2007, 249-264.

[5] Noel CE, Zhu F, Lee AY, Yanle H, Parikh PJ. "Segmentation precision of abdominal anatomy for MRI-based radiotherapy." Med Dosim, 2014, 39(3), 212–217.

[6] Rohlfing T, Brandt R, Menzel R, Maurer CR. "Evaluation of atlas selection strategies for atlas-based image segmentation with application to confocal microscopy images of bee brains." Neuroimage, 2004, 21, 1428–1442.

[7] Rohlfing T, Russakoff DB, Maurer CR Jr. "Performance-based classifier combination in atlas-based image segmentation using expectation-maximization parameter estimation." IEEE Transactions on Medical Imaging, 23(8): 983–994, Aug 2004.

[8] Rohlfing T, Maurer CR. "Multi-classifier framework for atlas-based image segmentation." Pat Rec Let, 2005, 26, 2070-2079.

[9] Iglesias J E, Sabuncu M R. "Multi-Atlas Segmentation of Biomedical Images: A Survey." Med Image Anal, 2015, 24(1), 205-219.

[10] Gupta V, Wang Y, Romero A, Myronenko A, Jordan P, Heijmen B, Hoogeman M, "SU-E-J-208: Fast and Accurate Auto-Segmentation of Abdominal Organs at Risk for Online Adaptive Radiotherapy." Med Phys, 2014, 41(6), 205.

[11] Vandemeulebroucke J, Rit S, Kybic J, Clarysse P and Sarrut D. "Spatiotemporal motion estimation for respiratory-correlated imaging of the lungs." Med Phys, 2011, 38(1), 166-178.

[12] Piper J, Duchateau M, Nelson A, Verellen D, De Ridder M, "Characterizing accuracy in 4DCT Deformable registration using the POPI Model." Med Phys, 2013, 40, 168.

[13] "Validation of Mirada's CT Deformable Image Registration." White Paper mm4430-0-USA, Mirada Medical, 2013.

[14] Brouwer CL, Steenbakkers RJHM, van den Heuvel E, Duppen JC, Navran A, Bijl HP, Chouvalova O, Burlage FR, Meertens H, Langendijk JA, van 't Veld AA. "3D Variation in delineation of head and neck organs at risk." Radiation Oncology, 2012, 7(32).

ACCURAY

UNITED STATES

Accuray Corporate Headquarters
1310 Chesapeake Terrace
Sunnyvale, CA 94089
USA
Tel: +1.408.716.4600
Toll Free: 1.888.522.3740
Fax: +1.408.716.4601
Email: sales@accuray.com

Accuray Incorporated
1240 Deming Way
Madison, WI 53717
USA
Tel: +1.608.824.2800
Fax: +1.608.824.2996

ASIA

Accuray Japan K.K.
Shin Otemachi Building 7F
2-2-1 Otemachi, Chiyoda-ku
Tokyo 100-0004
Japan
Tel: +81.3.6265.1526
Fax: +81.3.3272.6166

Accuray Asia Ltd.
16/F, Tower 5, The Gateway
Harbour City
15 Canton Road, T.S.T
Hong Kong
Tel: +852.2247.8688
Fax: : +852.2175.5799

Accuray Accelerator Technology (Chengdu) Co., Ltd.
No. 8, Kexin Road
Hi-Tech Zone (West Area)
Chengdu
611731 Sichuan
China

EUROPE

Accuray International Sarl
Route de la Longeraie 9
CH – 1110 Morges
Switzerland
Tel: +41.21.545.9500
Fax: +41.21.545.9501

Important Safety Information:
Most side effects of radiotherapy, including radiotherapy delivered with Accuray systems, are mild and temporary, often involving fatigue, nausea, and skin irritation. Side effects can be severe, however, leading to pain, alterations in normal body functions (for example, urinary or salivary function), deterioration of quality of life, permanent injury, and even death. Side effects can occur during or shortly after radiation treatment or in the months and years following radiation. The nature and severity of side effects depend on many factors, including the size and location of the treated tumor, the treatment technique (for example, the radiation dose), and the patient's general medical condition, to name a few. For more details about the side effects of your radiation therapy, and to see if treatment with an Accuray product is right for you, ask your doctor.

MKT-TxPlg-0917-0050